IEEE Access
Multidisciplinary ⋮ Rapid Review ⋮ Open Access Journal

Received May 5, 2022, accepted May 24, 2022, date of publication May 30, 2022, date of current version June 6, 2022.

Digital Object Identifier 10.1109/ACCESS.2022.3178993

Model Based Moving Horizon Optimal Modes-Switch Schedule in Hybrid Powertrains for Marine Applications

GIANMARIO RINALDI[1], **PRATHYUSH P. MENON**[1], **AND RICHARD CREEK**[1]
[1]Centre for Future Clean Mobility, University of Exeter Engineering Research Centre, Exeter EX5 2GD, U.K.

Corresponding author: Gianmario Rinaldi (g.rinaldi3@exeter.ac.uk)

This work was supported by Lynch Motors through the Innovative U.K. Project Knowledge Transfer Partnership (KTP) (115043).

ABSTRACT Nowadays, the hybridisation and the electrification of the powertrains for the marine sectors are of paramount importance to reduce their carbon footprints. In this paper, a novel method is proposed to schedule the modes-switch of an hybrid powertrain for marine applications. The considered system is composed of an Internal Combustion Engine mounted in parallel with a Lynch DC Brushed Electric Machine to deliver power at the propeller shaft. The two key-findings of this paper are: *i*) A compact mathematical representation of the powertrain to model the energy balances and switching of the different modes of operation. *ii*) A novel graph-inspired approach to determine the optimal operational mode sequence. The objective is to find the modes schedule over a fixed time horizon that minimises both the fuel consumed and the number of modes changes. The solution is motivated by both the moving horizon principle and the shortest path identification algorithm, and it also relies on a predictive information of the power cycle. Numerical simulations are undertaken, showing the benefits of the proposed scheme. The proposed method is convenient to scale up for the integration of additional energy storage components or new modes of operation.

INDEX TERMS Optimisation, hybrid powertrains, discrete-time systems.

I. INTRODUCTION

The marine and the shipping sectors are currently responsible for approximately 2.7% of the global CO_2 emissions [1]. Nonetheless, predictions have been made, revealing that these two sectors will produce 15% of the global CO_2 emissions by 2050 [2]. To counteract against these forecasts, policymakers, stakeholders and researchers are putting an unprecedented effort to propose and implement effective solutions to reduce the carbon footprint of marine and shipping activities.

Conventionally, Diesel Internal Combustion Engines (ICEs) have been utilised to deliver propulsion in marine and shipping sectors [3]. These powertrains have the potential to better perform to tighten the fuel consumption, the CO_2 emissions and also the operational costs (see [3], [4] and the references therein). Amongst the possible system integration strategies to reduce the carbon footprint, the electrification and the hybridisation of the powertrains have remarkably captured the attention of the scientific community [5]. The hybridisation process typically consists of integrating a battery storage system (BSS) with its battery management systems (BMS) and the electric motor in parallel with a pre-existing ICE-driven powertrain. Given this configuration, the hybrid system can work on different modes of operation, allowing the propeller shaft to be powered (partially or totally) by the electric motor. The ultimately goal of an hybrid powertrain is to force the ICE to operate at more efficient working points [6] to reduce the emissions and the fuel consumption. This can be satisfied, (when permitted by the physical constraints and by the current status of the powertrain), by selecting the best amongst the possible modes of operations such as [3], [6]: *i*) by sharing the power propeller demand between the electric motor and the ICE; *ii*) by disengaging the ICE and use exclusively the electric motor to deliver propulsion; *iii*) by using the ICE to both recharging the BSS and powering the propeller; *iv*) by recovery the energy from the propeller shaft during deceleration phases to recharge the BSS.

Unsurprisingly, the hybridisation of an ICE powertrain gives rise to unprecedented challenges in controlling the

The associate editor coordinating the review of this manuscript and approving it for publication was Christopher H. T. Lee.

powertrain components and in managing the energy flowing throughout the whole system. Whilst delivering the required mechanical power at the propeller shaft is a must, multiple conflicting goals need to be addressed. Specifically, it is essential to manage the BSS in a safe and reliable way, to minimise the ICE diesel consumption and the powertrain operational costs, and to maximise the components lifespans (see [7] where both the size and the energy management of an hybrid vessel has been investigated, or [8], where a Model Predictive Control (MPC)-inspired method has been conceived to minimise the total fuel consumption of an hybrid vehicle, and [9], where the goal was also to minimise the NO_x emissions).

II. LITERATURE REVIEW

Energy managements and modes-switch techniques have been revealed to be effective tools to control the hybrid powertrains for marine applications [3]. The underlying idea of such approaches is to select and update the mode of operation of the powertrain minimising the desired goals (i.e. the total diesel consumed) whilst satisfying constraints imposed by the power/energy balance at the propeller shaft and by the physics of the system [10]. As illustrated in [11], two key-approaches are utilised to achieve energy managements in hybrid powertrains. The first approach is the so-called regular control strategy, which is a basic scheme selecting the mode of operation depending upon a set of rules (i.e. the level of the State Of Charge (SOC) of the BSS and the power demand at the propeller shaft) [12]. This procedure, whilst easy to be implemented in an online fashion, it is not able to guarantee an optimised energy management strategy [13]. Conversely, in the model-based optimised energy management schemes [14], a mathematical model of the powertrain is made use of [6]. The model predicts the evolution of the powertrain over a selected time-frame [4], and an optimisation problem is solved online to determine the optimal control strategy of the system [15], which can be the optimal mode selection [16].

Different optimisation-based solutions have been proposed to address the energy management and the modes-shift problems in powertrains [17], such as MPC, [11], analytical convex optimisation algorithms [8] or even nature-inspired algorithms [18]. For example, in [19] a optimisation problem has been solved to minimise both the tracking error for the propeller power demand and the losses of the power systems. Similarly, in [20] the instantaneous fuel consumption has been minimised in real time. Optimal control principles have also been applied to full electric vessels comprising BSS and super-capacitors to regulate the SOC maximising the lifespan of the energy storage devices [21] and dealing with pulsing loads [22]. Optimisation methods have also been recently utilised for sizing of hybrid ships with ICE, BSS and fuel cells [23].

To the best of the authors' knowledge, relatively little attention has been paid so far to conceive model-based optimal modes-switch predictive schedule for hybrid powertrains in the marine sector. Inspired by the receding horizon control [24], which has been classically applied to solve optimal control problems [25]. an optimal mode switch strategy has been formulated in [10]. The selected cost function included the total fuel consumed and additional penalty costs for breaching the SOC reference of the BSS. Mode-shift schedules have also been conceived to minimise the kinetic energy difference of the components involved before and after the mode-shift [26]. Optimal mode schedule has been recently conceived in [27], with a primarily application to road powertrain. The core of this approach is the exploitation of predictions of the vehicle behaviour within a future time horizon to schedule the modes-switch.

Main Contribution:

This paper proposes a novel optimal real-time method to switch the modes of operation for an hybrid powertrain for marine applications. A marine powertrain composed of a ICE engine operating in parallel with a Lynch DC Brushed Electric Machine (LEM) is considered. The LEM is powered by a BSS and it can also operate as a generator for BSS charging. The substantial contributions of this study are summarised in two key-findings: *i*) *The derivation of an original model that compactly describes the energy balances of the powertrain for each mode of operation*. To achieve this objective, two state variables, namely the ICE instantaneous fuel consumption and the SOC of the BSS are introduced. For each mode of operation, energy balances, speed relations and constrained are presented and a set of discrete-time equations are utilised to map the evolution of the two aforementioned state variables. In addition, inspired by the binary modes variables and matrices [28] a novel and compact discrete-time system is derived to model the energy balance of the powertrain.

ii) *The design a novel optimal predictive modes-switch schedule for the considered powertrain based on both the prediction of the power duty cycle and inspired by the shortest path algorithm for graphs*. The scheme is based on the model illustrated at point *i*) and it is inspired by the receding horizon technique [24] and by the shortest path search techniques for graphs [29]. Precisely, the prediction of the power duty cycle for the next τ_D hours is made use of. The τ_D hours time window is divided into r_{dc} time intervals of equal duration at the end of which the mode of the powertrain is permitted to switch. A modes-based graph [30] is created within the τ_D hours time, where each nodes corresponds to the mode of operation to select within each time interval, and the edges corresponds to the *weight* that the associated reached node bring. The weight here represents the value of the cost function to reach the selected mode and it accounts for both the fuel consumed to reach the node and the penalty factor associated with the mode changes. A r_{dc}-hop minimum weigh path search problem [29] is solved to identify the optimal list of modes to apply to the powertrain. Inspired by the receding horizon principle, only the *first* hop is applied and the movable time window is shifted.

The proposed method distinguishes from the existing ones, which are primarily applied to electric cars [27] and they

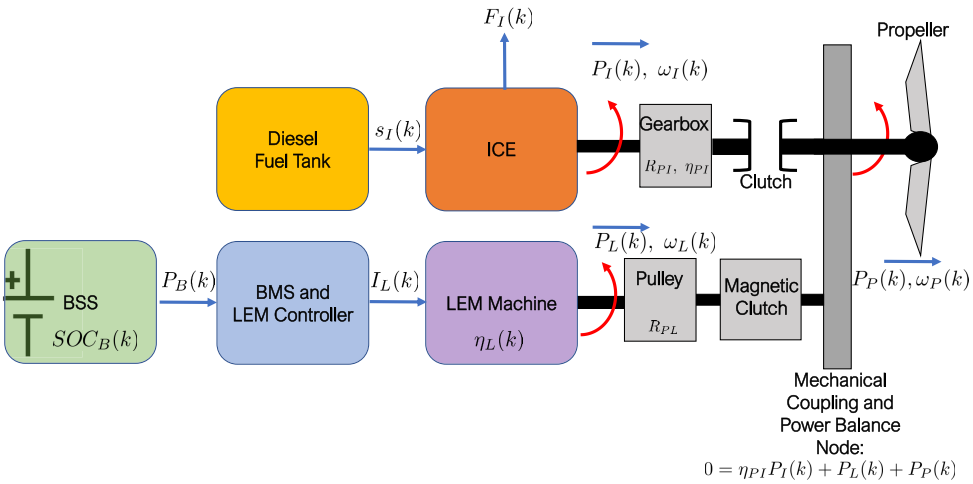

FIGURE 1. **The schematic of the considered hybrid powertrain. The arrowheads indicate the positive power sign convention.**

minimise the power tracking error [19], or to the lifespans of the BSS [21]. Ergo, to the best of the authors' knowledge, the proposed methodology inspired by binary matrix modelling and minimum weight path identification to to address energy management and modes-switch schedule for powertrains in marine sector is novel and it has never been proposed before. Furthermore, in this study it is shown that the adopted approach is easily adaptable to changes and upgrades to powertrains. Specifically, if new modes of operations become available, the model-based approach can incorporate them. Furthermore, if new energy storage devices (such as super capacitors or fuel cells) are included in the powertrain, the proposed methodology can still be applicable in such scenarios.

A. NOTATION

The notation adopted in this paper is standard. For a given discrete-time variable x, $x(k)$ denotes its value acquired at the time instant $k\Delta t$, where Δt is the sampling time. For a vector x, x^T denotes its transpose. For a set $\mathcal{X}$, the symbol $|\mathcal{X}|$ denotes its cardinality.

B. STRUCTURE OF THE PAPER

The rest of the present manuscript is structured as follows. Section III introduces the powertrain configuration and the operational modes. Section IV describes the considered powertrain components and the derivation of a compact model for the energy balance. Section V formulates the optimisation methodology and provides the design of the novel modes-switch schedule. Section VI presents the results undertaken to validate the effectiveness of the present study, whilst Section VII concludes the paper.

III. SYSTEM DESCRIPTION

A. POWERTRAIN CONFIGURATION

In this paper, a hybrid powertrain configuration is considered as depicted in Figure 1. The main components of the configuration are: *i*) An ICE to directly power the mechanical drive-train, *ii*) A LEM machine (with its BMS and motor controllers) operated in parallel with the main ICE drive shaft via an additional pulley, *iii*) A magnetic clutch to engage/disengage the LEM from pulley, *iv*) A clutch to engage/disengage the ICE from the pulley, and *v*) A BSS coupled with a BMS and LEM motor controller. The subscript I is adopted for the ICE engine, the subscript B is adopted for the battery pack and converter, the subscript L is adopted for the LEM machine, whilst the subscript P is adopted for the propeller. Table 1 lists the symbols and the variables adopted in the paper along with a brief description of their physical meaning.

Power Sign Convention:

The power at the propeller shaft is negative as consumed by this component, i.e. $P_P(k) < 0$. The output power at the ICE shaft is always positive $P_I(k) > 0$, as it is generated by this component. The output power at the LEM machine shaft is *positive*, i.e. $P_L(k) > 0$ if LEM functions as *motor*. Conversely, the output power at the LEM shaft is *negative*, i.e. $P_L(k) < 0$ if LEM functions as *generator*. The power flow between the different components is illustrated in Figure 1, where the arrowheads denote the positive power sign convention.

B. OPERATIONAL MODES

The hybrid powertrain configuration works in *three* possible modes. These modes are indicated as $\{\mathcal{M}_I, \mathcal{M}_L, \text{and } \mathcal{M}_{IL}\}$ respectively and discussed in sequel. Let N_M be the cardinality of the modes set, here fixed at 3. In order to formulate a compact mathematical representation of the three modes of operation following representation is introduced. Let the binary scalar variables $m_I(k)$ and $m_L(k)$ represents respectively the '`engage`(1)' and '`disengage` (0)' of the ICE clutch and of the LEM magnetic clutch with which the ICE and LEM operations in the configuration can be selected.

TABLE 1. List of symbols and variables adopted in the paper.

Symbols and Units	Meaning
ICE:	
$s_I(k)$ (kg/s)	the instantaneous ICE fuel consumption
$F_I(k)$ (kg)	the total fuel consumed by the ICE
$P_I(k)$ (kW)	the output power at the ICE shaft
$T_I(k)$ (Nm)	the torque at the ICE shaft
$SFC_I(k)$ (g/kWh)	the specific fuel consumption of the ICE
$\omega_I(k)$ (rad/s)	the speed at the ICE shaft
$\eta_I(k)$	the efficiency of the ICE
$P_{Imin} = 4$ (kW)	minimum ICE power
$P_{Imax} = 40$ (kW)	maximum ICE power
$\omega_{Imin} = 300$ (RPM)	minimum ICE speed
$\omega_{Imax} = 4000$ (RPM)	maximum ICE speed
$R_{PI} = 3$	the gearbox ratio
$\eta_{PI} = 0.90$	the efficiency of the gearbox
ine	
BSS and Machine Controller:	
$E_B(k)$ (kWh)	the energy stored in the BSS
$P_B(k)$ (kW)	the power flowing in (−) or out (+) the BSS
$SOC_B(k) := E_B(k)/E_B^M$	the state of charge of the BSS
$E_B^M = 15$ (kWh)	the maximum energy that can be stored in the BSS
$\eta_B = 0.92$	the efficiency of the BSS
$SOC_{Bmin} = 0.20$	minimum BSS SOC
$SOC_{Bmax} = 0.90$	maximum BSS SOC
ine	
LEM Machine:	
$V_L(k)$ (V)	the armature voltage of the LEM machine
$I_L(k)$ (A)	the armature current of the LEM machine
$P_L(k)$ (kW)	the output power of the LEM machine
$\omega_L(k)$ (rad/s)	the speed at the LEM shaft
$T_L(k)$ (Nm)	the torque at the LEM shaft
$\eta_L(k)$	the efficiency of the LEM machine
$P_{Lmax} = 10.50$ (kW)	LEM maximum power
$\omega_{Lmax} = 3648$ (RPM)	LEM maximum speed
$R_{PL} = 3$	LEM pulley ratio
ine	
Propeller:	
$P_P(k)$ (kW)	the power at the propeller shaft
$\omega_P(k)$ (rad/s)	the speed at the propeller shaft

Define a mode binary matrix at the time instant $k\Delta t$, $\mathcal{M}(k)$, as

$$\mathcal{M}(k) := \begin{bmatrix} m_I(k) & 0 \\ 0 & m_L(k) \end{bmatrix}, \tag{1}$$

and the mode dependent parameters $f_1(M(k))$ and $f_2(M(k))$ as

$$f_1(\mathcal{M}(k)) := \Big(m_L(k) - m_I(k)\Big)m_L(k), \tag{2}$$

$$f_2(\mathcal{M}(k)) := m_I(k)m_L(k). \tag{3}$$

Making use of (1)-(3), three operational modes $\mathcal{M}_I$, $\mathcal{M}_L$ and $\mathcal{M}_{IL}$ of the powertrain are:

1 Mode $\mathcal{M}_I$: The magnetic clutch is `disengage` (i.e., $m_L = 0$), the LEM machine is off, and the propulsion is provided entirely by the ICE. Hence, $m_I = 1$ and the mode matrix and dependent parameters are

$$\mathcal{M}(k) = \begin{bmatrix} 1 & 0 \\ 0 & 0 \end{bmatrix} =: \mathcal{M}_I, \tag{4}$$

$$f_1(\mathcal{M}(k)) = 0, \tag{5}$$

$$f_2(\mathcal{M}(k)) = 0. \tag{6}$$

2 Mode $\mathcal{M}_L$: The magnetic clutch is `engaged` (i.e., $m_L = 1$) and the propulsion is provided by the LEM machine, and the ICE is off (Hence, $m_I = 0$). The mode matrix and dependent parameters for the LEM alone mode are

$$\mathcal{M}(k) = \begin{bmatrix} 0 & 0 \\ 0 & 1 \end{bmatrix} =: \mathcal{M}_L, \tag{7}$$

$$f_1(\mathcal{M}(k)) = 1, \tag{8}$$

$$f_2(\mathcal{M}(k)) = 0. \tag{9}$$

3 Mode $\mathcal{M}_{IL}$: The ICE provides the propulsion at the propeller shaft and it drives the LEM machine as generator to recharge the BSS. Hence $m_I(k)$ and $m_L(k)$ are set to 1 and the mode matrix and dependent parameters while ICE and LEM are operated together are

$$\mathcal{M}(k) = \begin{bmatrix} 1 & 0 \\ 0 & 1 \end{bmatrix} =: \mathcal{M}_{IL}, \tag{10}$$

$$f_1(\mathcal{M}(k)) = 0, \tag{11}$$

$$f_2(\mathcal{M}(k)) = 1. \tag{12}$$

IV. POWERTRAIN MODEL

This sections describes the model of each component of the powertrain. For the purpose of developing the energy

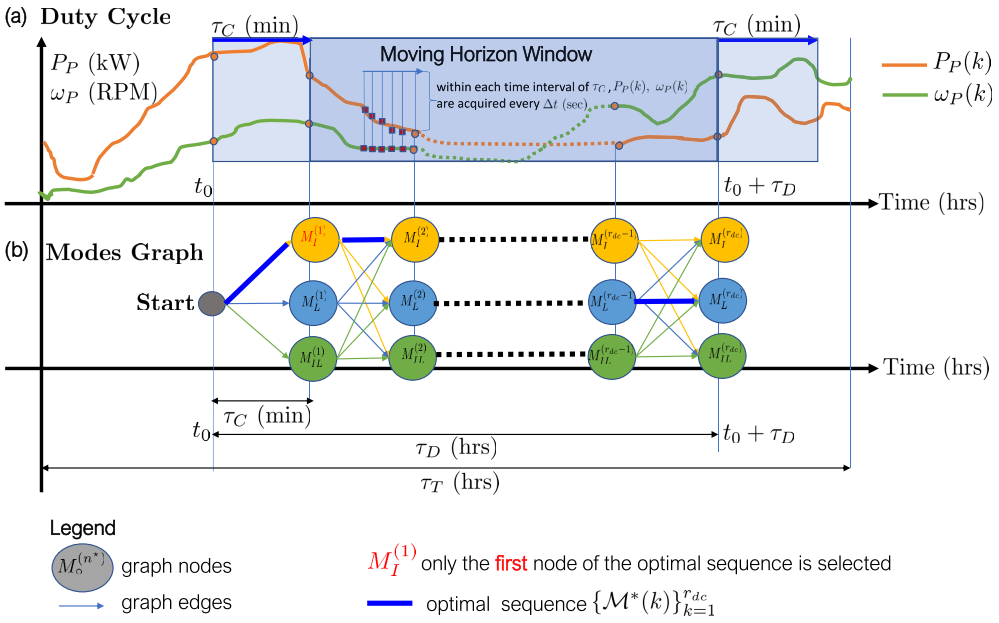

FIGURE 2. **(a): The time histories of the propeller power demand $P_P(k)$ and speed $\omega_P(k)$ along with the moving time window for the optimisation. (b): The modes graph along with the optimal minimum weight path.**

management solution, a compact discrete-time dynamical model is also derived. This model captures the changes amongst the three modes of operation described in Section III.

Assumptions:

In this study, the following assumptions are imposed

Assumption 1:(**A1**) The power and the speed at the propeller shaft defining the power duty cycle is assumed to be bounded, i.e.

$$|P_P(k)| < P_{Pmax}, \quad \forall k, \tag{13}$$
$$|\omega_P(k)| < \omega_{Pmax}, \quad \forall k, \tag{14}$$

where P_{Pmax} and ω_{Pmax} are known positive constants.

(A2) The maximum power of the ICE is P_{Imax} and it is assumed that the condition

$$P_{Imax} > P_{Pmax}, \tag{15}$$

holds.

Note that Assumption 1-(A2) ensures that the ICE is able to deliver, if required by the duty cycle, any power at the propeller shaft within the range $[0, P_{Imax}]$.

A. ICE MODEL

The instantaneous fuel consumption of the ICE is denoted by the variable $s_I(k)$, measured in (kg/s). For each pair $(P_I(k), \omega_I(k))$ it is possible to determine the instantaneous value of the fuel consumption using a numerical map $h_I((P_I(k), \omega_I(k))$. The total fuel consumed by the ICE up to the time instant $(k+1)\Delta t$ is obtained via a discrete-time integrator. Therefore, the ICE Model can be shown to be [31]:

$$s_I(k) = h_I(P_I(k), \omega_I(k)) \tag{16a}$$
$$F_I(k+1) = F_I(k) + s_I(k)\Delta t \tag{16b}$$
$$F_I(0) = F_{I0} \tag{16c}$$

The initial condition (16c) is typically set as $F_{I0} = 0$. The working region of the ICE is limited by the following constraints on the output power $P_I(k)$ and speed $\omega_I(k)$:

$$P_{Imin} < P_I(k) < P_{Imax} \tag{16d}$$
$$\omega_{Imin} < \omega_I(k) < \omega_{Imax} \tag{16e}$$

where P_{Imin} and P_{Imax} are respectively the minimum and the maximum ICE output power, whilst ω_{Imin} and ω_{Imax} are respectively the minimum and the maximum ICE speed.

B. LEM MACHINE MODEL

The LEM machine is modelled using its steady-state characteristics [32]. In particular, it is possible to measure the output power $P_L(k)$ and the speed at the LEM machine shaft, $\omega_L(k)$. Since $P_L(k)$ and $\omega_L(k)$ measurements are available, the armature voltage $V_L(k)$, the input current to the motor $I_L(k)$, and the efficiency of the machine $\eta_L(k)$ can be determined by direct numerical interpolation using the technical data curves available in [32], which is made available as a look up table. At the core of the proposed optimal modes-switch schedule there is the interpolating map of the efficiency of the LEM, which is [32]:

$$\eta_L(k) = f_{\eta_L}(P_L(k), \omega_L(k)). \tag{17a}$$

The working region of the LEM machine is bounded by both power and speed constraints:

$$-P_{Lmax} < P_L(k) < P_{Lmax} \tag{17b}$$
$$0 < \omega_L(k) < \omega_{Lmax} \tag{17c}$$

where P_{Lmax} and ω_{Lmax} are positive constant and they represent respectively the maximum power and speed of the LEM machine. Note that the power constraint (17b) explicitly allows the LEM machine to function as generator whenever $P_L(k) < 0$ (under the power convention adopted in this study).

C. BSS MODEL

The battery pack is modelled as a discrete-time dynamical system describing the time evolution of its (SOC_B). Inspired by the dynamics of SOC reported in the literature [3], [5], [31], [33], [34], for a three-modes powertrain system, the dynamics of SOC_B is given by [31]:

$$SOC_B(k+1) = \begin{cases} SOC_B(k), & \mathcal{M}_I \\ SOC_B(k) - \dfrac{P_L(k)}{\eta_L(k)\eta_B E_B^M}\Delta t, & \mathcal{M}_L \\ SOC_B(k) - \dfrac{\eta_L(k)\eta_B P_L(k)}{E_B^M}\Delta t, & \mathcal{M}_{IL} \end{cases} \tag{18a}$$

$$SOC_B(0) = SOC_{B0} \tag{18b}$$

Note that, differently from [31], [34], the proposed dynamics of BSS accounts for three different modes of operation of the powertrain. Furthermore, the efficiency of the BSS converter η_B and the (time-varying) efficiency of the LEM machine $\eta_L(k)$, are explicitly accounted for the charging/discharging processes of the BSS. Three equations in (18a) describes the changes to the state of charge of the battery pack in three different modes. In mode $\mathcal{M}_I$, the dynamics is considered as a pure discrete integrator. Whenever the LEM is functioning as motor ($\mathcal{M}_L$), i.e. $P_L(k) > 0$, the battery pack is discharging ($SOC_B(k+1)$ decreases from $SOC_B(k)$ in (18a)). Conversely, whenever the LEM is functioning as generator which occurs in $\mathcal{M}_{IL}$, the term $P_L(k)$ is negative according to the power sign convention described in Sec III. Henceforth, there is an increase in the charge of the battery back ($SOC_B(k+1)$ is larger than $SOC_B(k)$ in (18a)). As the LEM machine output power $P_L(k)$ flows in opposite directions during the charging/discharging processes, the efficiencies product $\eta_L(k)\eta_B$ appears at the denominator when the BSS is discharging (mode $\mathcal{M}_L$), whilst it appear at the numerator when the BSS is charging (mode $\mathcal{M}_{IL}$). The system in equations (18a) is subject to the initial condition as given in (18b). The operational regime of the battery pack follows the bound constraints on SOC_B:

$$SOC_{Bmin} < SOC_B(k) < SOC_{Bmax} \tag{18c}$$

where SOC_{Bmin} and SOC_{Bmax} represent respectively the prescribed minimum and maximum level of SOC_B.

D. POWER AND SPEED AT THE PROPELLER SHAFT

The power at the propeller shaft $P_P(k)$ and the the speed $\omega_P(k)$ are predicted over the time period of τ_D hours (see Figure 2). This set of data is assumed to be available every $k\Delta t$ seconds.

The torque at the propeller shaft can be retrieved as $T_P(k) = P_P(k)/\omega_P(k)$. Therefore, it is possible to write the following power balances:

$$0 = \begin{cases} \eta_{PI}P_I(k) + P_P(k) & \mathcal{M}_I \\ P_L(k) + P_P(k) & \mathcal{M}_L \\ \eta_{PI}P_I(k) + P_L(k) + P_P(k) & \mathcal{M}_{IL} \end{cases} \tag{19}$$

Analogously, it is possible to write the following speed relationships, which are also dictated by the parallel hybrid configuration in Figure 1.

$$0 = \begin{cases} \omega_I(k) - R_{PI}\omega_P(k) & \mathcal{M}_I \\ \omega_L(k) - R_{PL}\omega_P(k) & \mathcal{M}_L \\ \omega_I(k) - R_{PI}\omega_P(k) & \mathcal{M}_{IL} \\ \omega_L(k) - R_{PL}\omega_P(k) \end{cases} \tag{20}$$

Note that the last equation of the system in (20) represents the speed balance relations for the mode $\mathcal{M}_{IL}$, where both the ICE and the LEM are running in parallel (as depicted in Figure 1).

E. COMPACT REPRESENTATION

Given the set of equations of the ICE (16a)-(16c), the LEM machine (17a), the battery pack (18a), the power balances (19), and the speed relations (20), the dynamics of the hybrid powertrain can be written in the form of a discrete-time model as

$$x(k+1) = Ax(k) + B_P\delta(k)u(k)\Delta t \tag{21a}$$
$$x(0) = x_0 \tag{21b}$$
$$0 = E_P(\mathcal{M}(k))P(k) \tag{21c}$$
$$0 = \mathcal{M}(k)\tilde{\omega}(k) \tag{21d}$$

where the introduced variables and matrices are:

$$x(k) := \left[F_I(k)\ SOC_B(k)\right]^T \tag{21e}$$
$$x_0 := \left[F_{I0}\ SOC_{B0}\right]^T \tag{21f}$$
$$P(k) := \left[P_I(k)\ P_L(k)\ P_P(k)\right]^T \tag{21g}$$
$$\omega(k) := \left[\omega_I(k)\ \omega_L(k)\right]^T \tag{21h}$$
$$\tilde{\omega}(k) := \left[\omega_I(k) - R_{PI}\omega_P(k)\ \omega_L(k) - R_{PL}\omega_P(k)\right]^T \tag{21i}$$
$$A := \begin{bmatrix} 1 & 0 \\ 0 & 1 \end{bmatrix} \tag{21j}$$
$$B_P := B_{P_1}B_{P_2} = \underbrace{\begin{bmatrix} 1 & 0 & 0 \\ 0 & 1 & 1 \end{bmatrix}}_{B_{P_1}} \underbrace{\begin{bmatrix} 1 & 0 & 0 \\ 0 & -\dfrac{1}{\eta_B E_B^M} & 0 \\ 0 & 0 & -\dfrac{\eta_B}{E_B^M} \end{bmatrix}}_{B_{P_2}} \tag{21k}$$
$$\delta(k) := \begin{bmatrix} h_I(P_I(k), \omega_I(k)) & 0 & 0 \\ 0 & \dfrac{P_L(k)}{\eta_L(k)} & 0 \\ 0 & 0 & \eta_L(k)P_L(k) \end{bmatrix} \tag{21l}$$

$$u(k) := \begin{bmatrix} 1 \\ f_1(\mathcal{M}(k)) \\ f_2(\mathcal{M}(k)) \end{bmatrix} \tag{21m}$$

$$E_P(\mathcal{M}(k)) := \begin{bmatrix} \eta_{PI} m_I(k) \; m_L(k) \; 1 \end{bmatrix} \tag{21n}$$

Various bound constraints on ICE (16d)-(16e), on the LEM (17b)-(17c), and on the BSS (18c) described before hold here. Under the notation of the compact model (21a), these yield

$$x_{min} < x(k) < x_{max} \tag{22a}$$

$$P_{min} < P(k) < P_{max} \tag{22b}$$

$$\omega_{min} < \omega(k) < \omega_{max} \tag{22c}$$

where the introduced vectors are defined as:

$$x_{min} := \begin{bmatrix} 0 \; SOC_{Bmin} \end{bmatrix}^T \tag{22d}$$

$$x_{max} := \begin{bmatrix} +\infty \; SOC_{Bmax} \end{bmatrix}^T \tag{22e}$$

$$P_{min} := \begin{bmatrix} P_{Imin} \; -P_{Lmax} \end{bmatrix} \tag{22f}$$

$$P_{max} := \begin{bmatrix} P_{Imax} \; P_{Lmax} \end{bmatrix}^T \tag{22g}$$

$$\omega_{min} := \begin{bmatrix} \omega_{Imin} \; 0 \end{bmatrix}^T \tag{22h}$$

$$\omega_{max} := \begin{bmatrix} \omega_{Imax} \; \omega_{Lmax} \end{bmatrix}^T \tag{22i}$$

V. SCHEDULING MODES OF POWERTRAIN

The objective is to determine the optimal 'minimal' schedule of modes among $\{\mathcal{M}_I,\ \mathcal{M}_L,\ \mathcal{M}_{IL}\}$ that minimises the total energy consumption over a finite time horizon $[t_0,\ t_0 + \tau_D)$ based on a sampling at every τ_C minutes. The definition of 'minimal' schedule is to limit the number of consecutive mode changes that can occur at every τ_C minutes to a minimum number. The modes-switch frequency should be maintained below a minimum level to both limit the transient behaviour of the powertrain and to avoid frequent engines on/off compromising their lifespans [26]

Let t_0 be an arbitrary starting time and τ_D be the duration of the moving horizon time window in steps of τ_C minutes. It is assumed that the mode change, if any, occurs only every τ_C minute interval. Two sampling indices, basically positive integers, r_{cp} and r_{dc} are defined as

$$r_{cp} = \frac{60\tau_C}{\Delta t}, \tag{23}$$

$$r_{dc} = \frac{60\tau_D}{\tau_C}. \tag{24}$$

This implies that over a finite time horizon $[t_0,\ t_0 + \tau_D)$ the aim is to determine the optimal sequence of modes $\{\mathcal{M}^*(k)\}_{k=1}^{r_{dc}}$. Given the definition of r_{cp} and r_{dc}, the moving horizon of duration τ_D will have H_D number of sampling instances of measurements as $H_D = r_{cp} r_{dc}$. Similar to other predictive control methods [35], only the first value of the mode sequence $\{\mathcal{M}^*(k)\}_{k=1}^{r_{dc}}$ is actually employed and used in the real-time drive cycle control algorithm. After τ_C units of time, a new time horizon $[t_0 + \tau_C, t_0 + \tau_C + \tau_D)$ is considered and the whole optimisation process is repeated to generate a new sequence of modes by solving the optimisation with new initial conditions based on updated measurements at time $t_0 + \tau_C$. The mode switch is therefore only permitted every τ_C minutes. This imply, at every sampling instance, the operational mode is

$$\mathcal{M}(k+1) = \mathcal{M}^*(k), \;\; \text{if } k \neq j r_{cp}, \;\; \forall j = 0, \ldots, r_{dc} \tag{25}$$

where $\mathcal{M}^*(k) \in \{\mathcal{M}_I,\ \mathcal{M}_L,\ \mathcal{M}_{IL}\}$.

A. OPTIMISATION METHODOLOGY

A weighted directed acyclic graph based abstraction of the underlying process is considered. Let $\mathcal{G}(\mathcal{V}, \mathcal{E})$ be such a graph, where $\mathcal{V}$ is the set of vertices representing the mode of operation to be maintained during an interval of τ_C minutes. The vertices are named following the notation given in Figure 2. Let $n^\star$ be an integer satisfying $0 < n^\star < r_{dc}$, and introduce the auxiliary generic subscript '$\circ$' defining any selected mode amongst $\{\mathcal{M}_I, \mathcal{M}_L,$ and $\mathcal{M}_{IL}\}$. The vertex associated with the mode selected over the time period $(n^\star - 1) r_{cp} \Delta t \leq t < (n^\star) r_{cp} \Delta t$ is denoted by $M_\circ^{n^\star} \in \mathcal{V}$. The idea of finding the sequence of modes for traversing a distance during a time interval of τ_D becomes determining a *path* of length r_{dc} in a directed acyclic graph $\mathcal{G}$, i.e., a sequence of vertices $M_\circ^1 \sim M_\circ^2 \sim \cdots M_\circ^{n^\star} \sim \cdots M_\circ^{r_{dc}}$. The set of feasible paths connecting the vertices of the graph belongs to $\mathcal{E}$. An edge connects two neighbouring vertices $(M_\circ^{n^\star} \sim M_\circ^{n^\star+1})$ be defined as i.e., $M_\circ^{n^\star} \to M_\circ^{n^\star+1} \in \mathcal{E}$, note that the subscripts can be any among $\{I,\ L,\ IL\}$. In addition, let us define a positive weight function $\rho : \mathcal{E} \to J$ which associates each edge of the graph with a weight, which is defined depending on the fuel consumed and a cost associated with the mode change, described in sequel.

Let

$$z(k) = \begin{cases} 0 & \text{if } \mathcal{M}(k) = \mathcal{M}(k-1), \\ 1 & \text{else,} \end{cases} \tag{26}$$

tracks the occurrence of change of mode. Let

$$\mathcal{C}_F(k) = \frac{s_I(k)}{S_I}, \tag{27a}$$

$$\mathcal{C}_O(k) = z(k), \tag{27b}$$

where $\mathcal{C}_F(k)$ accounts for the cost of the fuel consumed, whilst $\mathcal{C}_O(k)$ represents the cost associated with alteration of mode-switch. The positive parameter S_I in (27a) represents the maximum possible value of the fuel consumption, which is retrieved from the ICE data-sheets. By combining (27a) and (27b), define a function

$$J(x(k), z(k)) := \lambda_F \mathcal{C}_F(k) + \lambda_O \mathcal{C}_O(k), \tag{28}$$

where λ_F and λ_O are positive scalar weighting factors.

Hence, the weight ρ associated with the directed edge $M_\circ^{n^\star} \to M_\circ^{n^\star+1} \in \mathcal{E}$ becomes

$$\rho\left(M_\circ^{(n^\star)} \to M_\circ^{(n^\star+1)}\right) := \sum_{k=r_{cp} n^\star}^{k=r_{cp}\cdot(n^\star+1)-1} J(x(k), z(k)). \tag{29a}$$

$$\left.\begin{aligned} &\text{where}\\ x(k+1) &= Ax(k) + B_P\delta(k)u(k)\Delta t\\ x(0) &= x(k = r_{cp}n^\star - 1)\\ 0 &= E_P(\mathcal{M}_\circ)P(k)\\ 0 &= \mathcal{M}_\circ\tilde{\omega}(k)\\ \mathcal{M}(k+1) &= \mathcal{M}(k) = \mathcal{M}_\circ\\ \mathcal{M}_\circ &\in \{\mathcal{M}_I,\ \mathcal{M}_L,\ \mathcal{M}_{IL}\} \end{aligned}\right\} \forall k, \tag{29b}$$

Likewise, the weight of other possible edges among other vertices can be determined. Therefore, the objective is to determine an optimal sequences of modes for the drive over the finite horizon $[t_0, t_0 + \tau_D)$ by minimising a finite horizon objective:

$$\{\mathcal{M}^*(k)\}_{k=1}^{r_{dc}} := \arg \min_{\{\mathcal{M}^*(k)\}_{k=1}^{r_{dc}}} \left(\sum_{k=1}^{H_D-1} J(x(k), z(k)) \right), \tag{30a}$$

$$\left.\begin{aligned} &\text{sub. to.}\\ x(k+1) &= Ax(k) + B_P\delta(k)u(k)\Delta t\\ x(0) &= x_0\\ 0 &= E_P(\mathcal{M}_(k))P(k)\\ 0 &= \mathcal{M}(k)\tilde{\omega}(k)\\ \mathcal{M}(k+1) &= \mathcal{M}(k)\ \text{if}\ k \neq jr_{cp},\ \ \forall j=1,\ldots,r_{cp}\\ \mathcal{M}(k) &\in \{\mathcal{M}_I,\ \mathcal{M}_L,\ \mathcal{M}_{IL}\}\\ x_{min} &< x(k) < x_{max}\\ P_{min} &< P(k) < P_{max}\\ \omega_{min} &< \omega(k) < \omega_{max} \end{aligned}\right\} \forall k, \tag{30b}$$

where the right hand side of (30a), the sum of over a finite time horizon $[t_0,\ t_0 + \tau_D)$ of the function $J(x(i), z(i))$, represents the cost of paths of length r_{dc}. As evident from Figure 2, for three modes and r_{dc} hopes there exists $3^{(r_{dc})}$ possible paths. The optimisation problem defined (30a) subject to dynamics, initial condition, and state bound constraints defined in (30b) is solved to determine the minimum weight path composed by r_{dc} hopes. The problem is therefore in the form of a standard minimum-weight path search with r_{dc} hopes and it is solved using the Dijkstra's Algorithm [36], obtaining the optimal sequence $\{\mathcal{M}^*(k)\}_{k=1}^{r_{dc}}$. The problem has an exponential complexity and its computational load might increase significantly but, on a realistic horizon of few modes like here (i.e., 3), the number of nodes can be kept low and computationally solvable easily.

Remark 1: Note that under the current graph-based formulation, the selected mode matrix in (29b) corresponds to the graph node

$$M_\circ^{(n^\star+1)} \in \mathcal{V}. \tag{31}$$

Additionally, the extremes of the sum operator in (29a) appropriately correspond to the time interval

$$(n^\star)r_{cp}\Delta t \leq t < (n^\star + 1)r_{cp}\Delta t. \tag{32}$$

Remark 2: If the evolution of the states $x(i)$ and the input $P(i)$ and $\omega(i)$ breach the inequality constraints in (30b), automatically the edge interconnecting is labelled as *unfeasible* and therefore it cannot be included in the optimal minimum weight path.

VI. SIMULATION RESULTS

This section presents the results of the simulations undertaken to validate the effectiveness of the key-findings of the present study. The values of the model parameters, and the maximum powers and speeds of the ICE and the LEM are shown in Table 1. The maps of the LEM machine is shown in Figure 3, and they have been generated relying on the data sheets [32]. A time horizon of $T = 2$ hours is considered. The movable time window has a duration $\tau_D = 1$ hour, whilst the mode changes is permitted every $\tau_c = 15$ minutes. The predictions of the power duty cycle are available with a sampling time of $\tau_P = 10$ seconds. It follows that they key-quantity for the graph-based optimal energy management in equations (23)-(24) are $r_{cp} = 90$, $r_{cp} = 4$, and $H_D = 360$.

Four Scenarios are introduced

- **Scenario 1**: in which both the propeller power speed and power remain constant, i.e. $P_P(k) = 4$ (kW) and $\omega_P(k) = 1200$ (RPM).
- **Scenario 2**: in which the propeller power remains constant, i.e. $P_P(k) = 4$ (kW) whilst the propeller speed $\omega_P(k)$ decreases linearly.
- **Scenario 3**: in which both the propeller power and speed are time-varying. Specifically, two level of power and speed at the propeller shaft are considered. A cruising speed-power pair

$$P_{Pn} = 6\ (\text{kW}) \tag{33}$$
$$\omega_{Pn} = 1000\ (\text{RPM}) \tag{34}$$

  and a high speed-power pair

$$P_{PM} = 12\ (\text{kW}) \tag{35}$$
$$\omega_{PM} = 1200\ (\text{RPM}) \tag{36}$$

- **Scenario 4:** in which the propeller power and speed are time-varying and they represent real data recorded during a vessel operation.[1] The time history of the power and speed cycle are depicted in Figure 7 (a)-(b).

For each scenario, two powertrain set-ups are considered:

- **(DO)**: "(Diesel Only)", in which the powertrain is forced to work only on the mode $\mathcal{M}_I$ in (4)
- **(OS)**: "(Optimal Solution)", in which the powertrain energy management strategy is governed by the proposed optimal graph-based approach.

For the two set-points **(DO)** and **(OS)**, the total fuel consumed by the ICE is respectively denoted with the notation $F_I^{(DO)}$ and $F_I^{(OS)}$. The metric (measured in percentage)

$$\Delta F_I := \frac{F_I^{(OS)} - F_I^{(DO)}}{F_I^{(DO)}} \tag{37}$$

is also introduced to compactly display the fuel saving using the proposed modes-switch schedule.

[1]The authors have been used the data recorded within the Innovative UK Project ISCF SBRI Phase 1, 115196: Option For Clean Propulsion Retrofit in Crew Transfer Vessel.

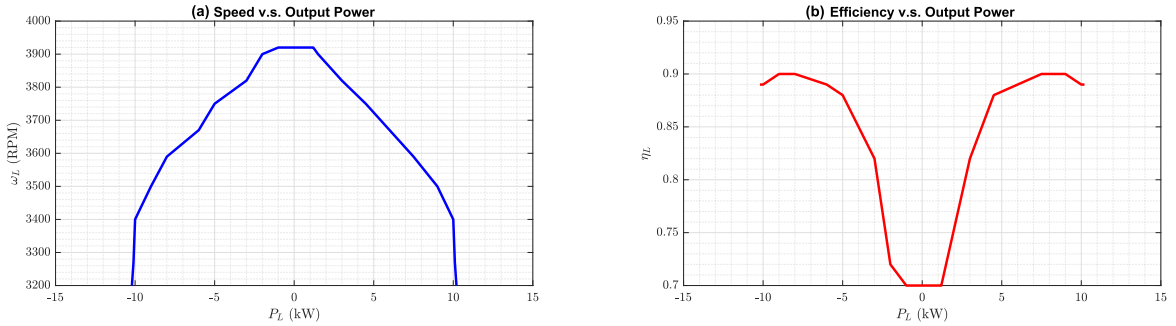

FIGURE 3. (a): The map representing the speed of the LEM machine ω_L as function of the output power P_L. (b): The map representing the efficiency of the LEM machine η_L as function of the output power P_L. The data are taken from [32].

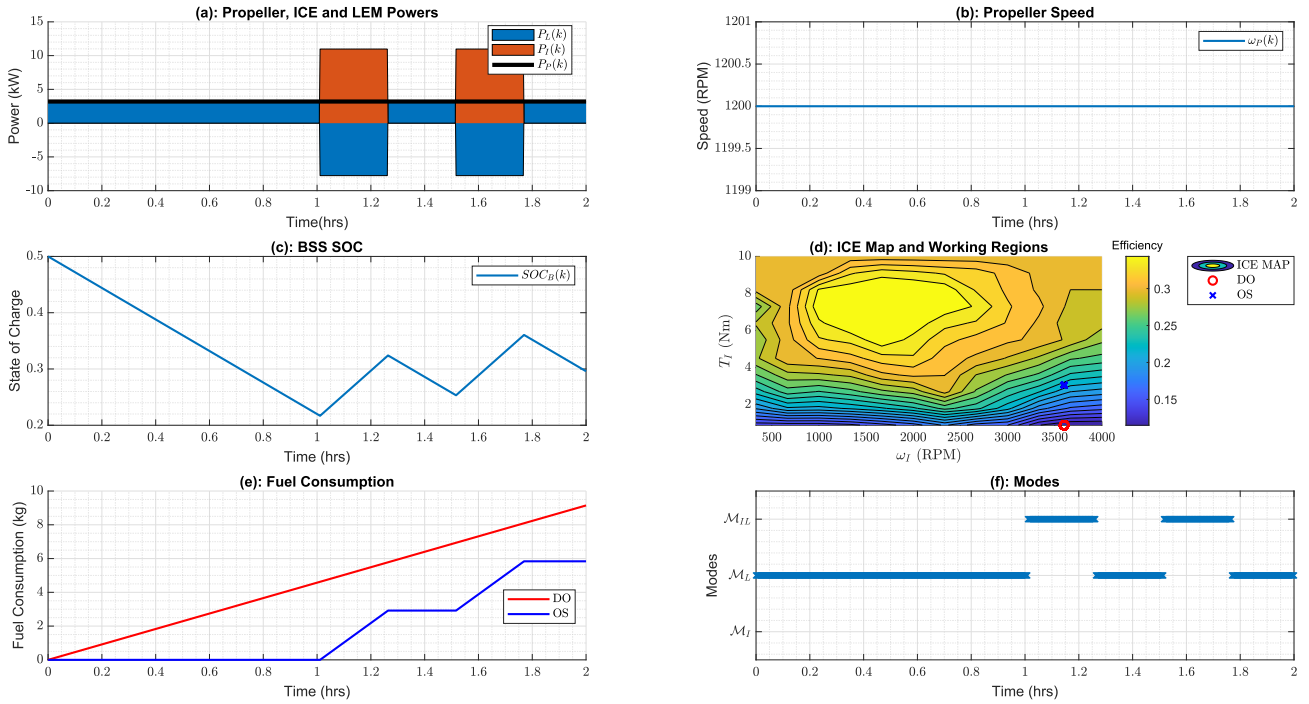

FIGURE 4. Scenario 1 Time histories of: (a): total power balances ($P_P(k)$, $P_I(k)$, $P_L(k)$), (b): propeller speed ($\omega_P(k)$), (c): BSS state of charge ($SOC_B(k)$), (d): ICE map with the working points for DO and OS set-ups, (e): total fuel consumption ($F_i(k)$) for DO and OS set-ups, and (f): optimal modes-switch schedule.

A. SCENARIO 1

During Scenario 1, the power duty cycle is characterised by a low power demand at a high speed (Figure 4-(a) and 4-(b)). The performances of the ICE in the DO setup are extremely inefficient. To support this, it is possible to determine the ICE efficiency from the contour map in Figure 4-(d), which is equal to $\approx$ 10%. A total amount of 9.12 kg of diesel are required to generate the required power at the propeller shaft. The powertrain better performs by functioning according to the proposed modes-switch schedule (OS setup). By applying a combination of modes $\mathcal{M}_L$ and $\mathcal{M}_{IL}$ (Figure 4-(f)), the proposed scheme provides to alternate. When the ICE is on, its efficiency is **22%**, which is much higher than **10%**. Note that the constraints on the SOC of the BSS are matched also, hence the proposed scheme implement periodic charging (see Figure 4-(c)). According to Table 2, the fuel consumption can be abated by more than **36%**.

B. SCENARIO 2

During Scenario 2, the propeller power remains constant, whilst the speed decrease linearly over time (Figure 5-(a)-(b)). Considerations analogous to Scenario 1 can be made. Specifically, in the **OS** setup, charging opportunities for the BSS are still captured (Figure 5-(f), and nearly **43%** of the fuel can be saved (Table 2). Note also that the ICE efficiency for the DO setup reaches a minimum below **10%**, whilst for the OS setup it passes **30%**.

C. SCENARIO 3

During Scenario 3, both the propeller speed and power are time-varying (Figure 6-(a)-(b)). Specifically, over the considered 2 hours period, the vessel spends most of its time at a "cruising speed" (i.e. $\omega_P(k) = 1000$ (RPM) and $P_P(k) = 6$ (kW)) with some short periods of "high speed"(i.e. $\omega_P(k) = 1200$ (RPM) and $P_P(k) = 12$ (kW)), 15 minutes at a

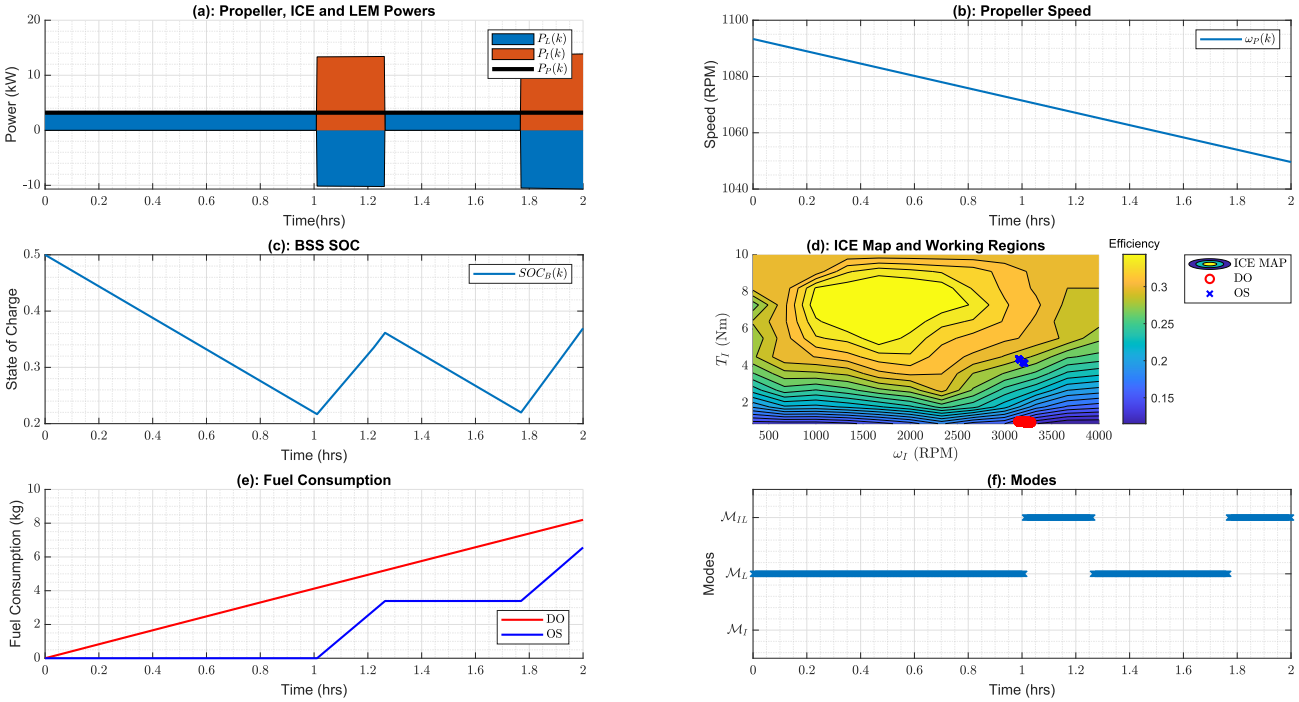

FIGURE 5. Scenario 2 Time histories of: (a): total power balances ($P_P(k)$, $P_I(k)$, $P_L(k)$), (b): propeller speed ($\omega_P(k)$), (c): BSS state of charge ($SOC_B(k)$), (d): ICE map with the working points for DO and OS set-ups, (e): total fuel consumption ($F_j(k)$) for DO and OS set-ups, and (f): optimal modes-switch schedule.

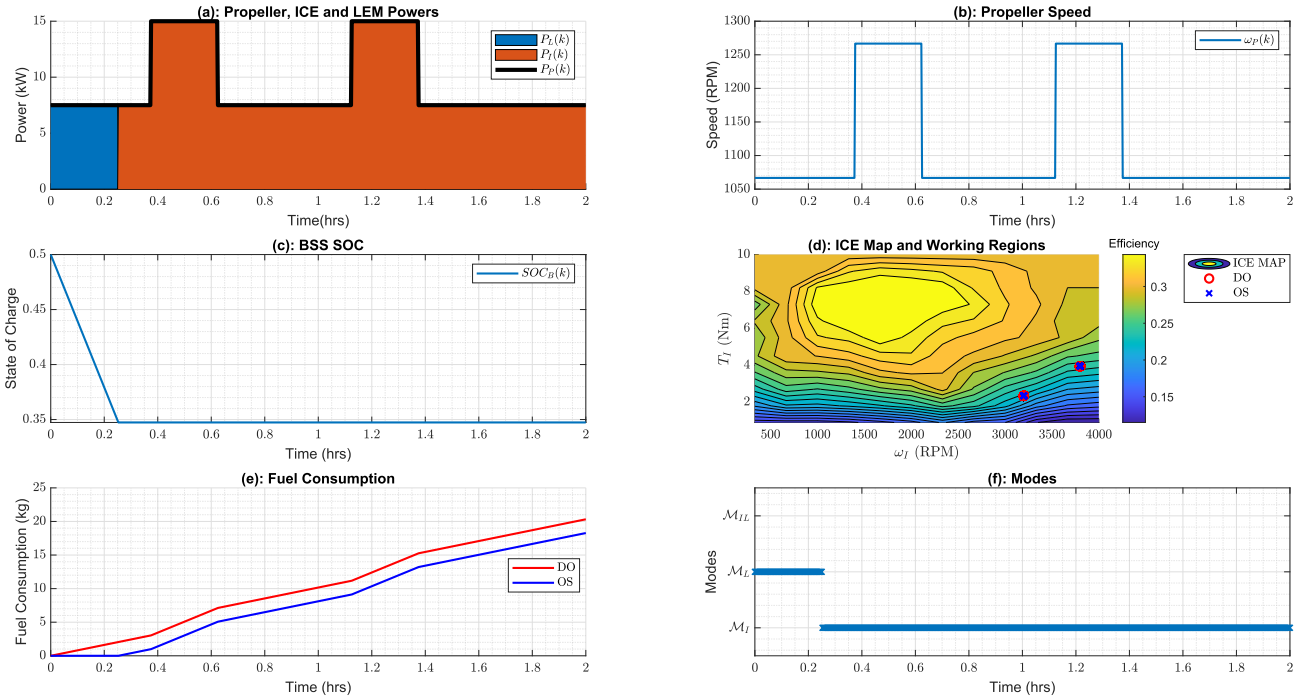

FIGURE 6. Scenario 3 Time histories of: (a): Total power balances ($P_P(k)$, $P_I(k)$, $P_L(k)$), (b): propeller speed ($\omega_P(k)$), (c): BSS state of charge ($SOC_B(k)$), (d): ICE map with the working points for DO and OS set-ups, (e): total fuel consumption ($F_j(k)$) for DO and OS set-ups, and (f): Optimal modes-switch schedule.

time. In this situation, the fuel consumption can be reduced by more than *20%* (Table 2), the proposed energy management strategy explores the modes $\mathcal{M}_I$ and $\mathcal{M}_L$ over the considered 2 hours time period (Figure 6-(f)). Furthermore, the BSS SOC constraints are still met (Figure 6-(c)).

Sensitivity Analysis to Power Variation for Scenario 3:

A sensitivity analysis can be undertaken considering variations of the power at the propeller shaft $P_P(k)$. Given the nominal parameters for the power at the propeller shaft (33) and (35), a parameters perturbation in the

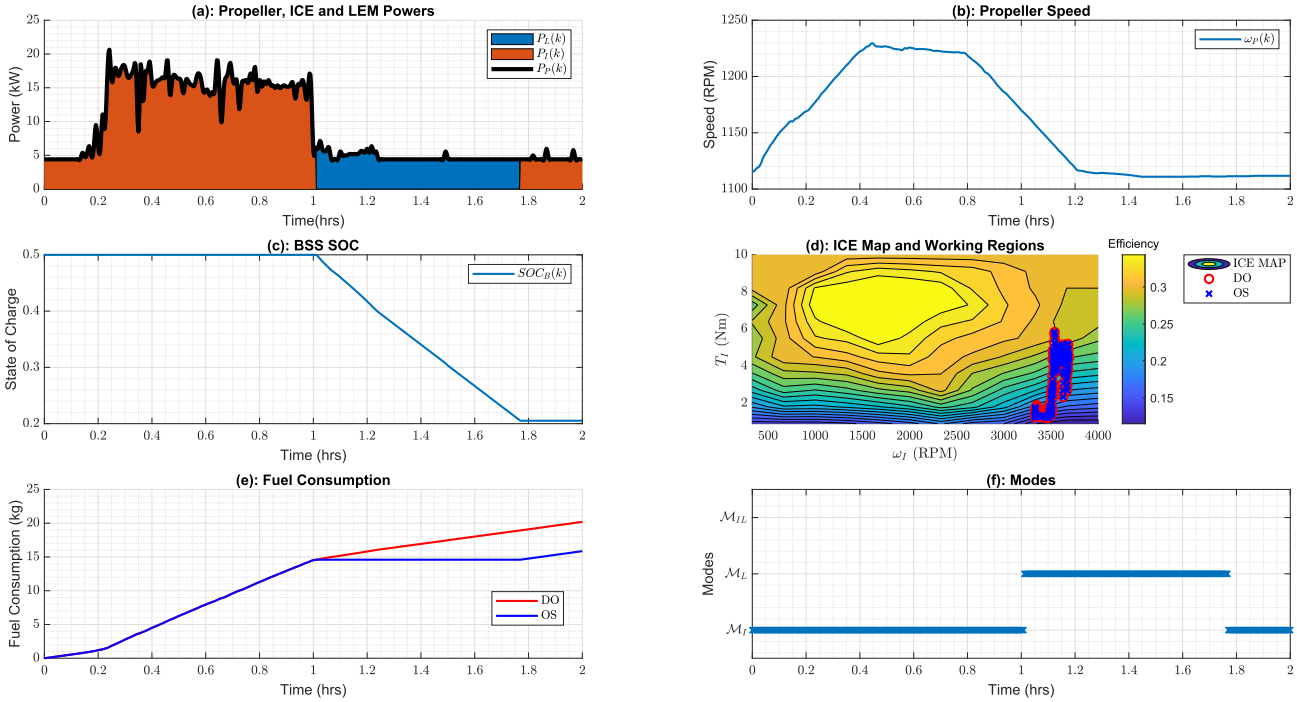

FIGURE 7. Scenario 4 Time histories of: (a): total power balances ($P_P(k)$, $P_I(k)$, $P_L(k)$), (b): propeller speed ($\omega_P(k)$), (c): BSS state of charge ($SOC_B(k)$), (d): ICE map with the working points for DO and OS set-ups, (e): total fuel consumption ($F_i(k)$) for DO and OS set-ups, and (f): optimal modes-switch schedul.

TABLE 2. The total fuel consumed for each scenario for the DO and the OS setups.

	Scen. 1	Scen. 2	Scen. 3	Scen. 4
$F_I^{(DO)}$(kg)	9.12	8.06	16.46	20.15
$F_I^{(OS)}$(kg)	5.83	4.62	13.08	15.84
ΔF_I (%)	**-36.07%**	**-42.68%**	**-20.53%**	**-21.39%**

form of

$$\tilde{P}_{Pn} = (1 + \delta P_P) P_{Pn} \tag{38}$$

$$\tilde{P}_{PM} = (1 + \delta P_P) P_{PM} \tag{39}$$

is considered, where δP_P is a parameter representing the variation. From the results reported in Table 3, two key-comments can be made. Firstly, the proposed scheme profitably works also under the considered sensitivity analysis given by (38)-(39). Secondly, it is noticeable that if the power propeller shaft drops, the fuel consumption can be abated by over **30%**.

D. SCENARIO 4

During Scenario 4, the proposed optimal modes-schedule scheme is tested by considering real power-speed cycle data shown in Figure 7 (a)-(b). The power/speed duty cycles here are characterised a first part, during the time interval [0,1] (hrs), in which the vessel is operating at high power/speed (power peak 20.63 (kW), speed peak 1230 (RPM)), with fluctuations, and a second part during the time interval [1,2] (hrs), in which the vessel is operating at a lower power/speed (power minimum 5 (kW), speed minimum 1110 (RPM)). During the first part, the mode $\mathcal{M}_I$ is made use of (Figure 7-(f)). When the power/speed decrease, the designed modes-switch schedule select the mode $\mathcal{M}_L$, until the minimum BSS SOC is reached (0.20). After this, for the remaining 15 minutes, the mode $\mathcal{M}_I$ is selected. Up to more than **21 %** of fuel can be saved also in this scenario.

TABLE 3. The total fuel consumed for Scenario 3, considering power variations of the duty cycle.

δP_P	$F_I^{(DO)}$(kg)	$F_I^{(OS)}$ (kg)	ΔF_I %
+25%	20.21	18.23	-9.80%
+20%	19.95	15.56	-22.01%
+15%	18.71	14.91	-20.31%
+10%	17.93	14.33	-20.08%
+5%	17.21	13.66	-20.63%
nominal	16.46	13.08	-20.53%
-5%	15.76	11.79	-25.19%
-10%	15.06	11.24	-25.37%
-15%	14.36	10.77	-25.00%
-20%	13.78	9.61	-30.26%
-25%	13.13	9.17	-30.16%

VII. CONCLUSION

In this paper, a novel graph-inspired method has been proposed to solve the modes-switch schedule problem in hybrid powertrains for marine application. An original compact mathematical representation of the energy flow throughout the powertrains component has been derived. In the derivation of the model, the binary algebra and variables have been

made use of. The solution addressing modes-switch schedule problem has been inspired by the moving horizon principle and by the graph-based approach to search for the minimum weight path. In such framework, the optimal path of the graph is the one minimising the fuel consumption and the modes-switch numbers. Detailed numerical simulations have been undertaken to validate the proposed methods, using prototypical data-sets. The benefits of modes-switch schedule have been demonstrated primarily considering the resulting fuel saving. In particular, it has been demonstrated that the designed modes-switch schedule have the potential to save up to 42 % (Scenario 3) of the fuel consumption by exploiting the modes selection. The use of recorded power/speed cycle data (Scenario 4) further demonstrated the applicability of the method. This study can be also considered a starting point for future research directions. For example, the designed scheme can be easily updated to incorporate additional clean powertrain components, such as hydrogen fuel cells and supercapacitors, or additional modes of operation.

ACKNOWLEDGMENT

The research data supporting this publication are provided within this paper.

REFERENCES

[1] Y. Zhang, S. D. Eastham, A. K. Lau, J. C. Fung, and N. E. Selin, "Global air quality and health impacts of domestic and international shipping," *Environ. Res. Lett.*, vol. 16, no. 8, Aug. 2021, Art. no. 084055.
[2] P. Serra and G. Fancello, "Towards the IMO's GHG goals: A critical overview of the perspectives and challenges of the main options for decarbonizing international shipping," *Sustainability*, vol. 12, no. 8, p. 3220, Apr. 2020.
[3] M. Jaurola, A. Hedin, S. Tikkanen, and K. Huhtala, "Optimising design and power management in energy-efficient marine vessel power systems: A literature review," *J. Mar. Eng. Technol.*, vol. 18, no. 2, pp. 92–101, 2018.
[4] H. P. Nguyen, A. T. Hoang, S. Nizetic, X. P. Nguyen, A. T. Le, C. N. Luong, V. D. Chu, and V. V. Pham, "The electric propulsion system as a green solution for management strategy of CO_2 emission in ocean shipping: A comprehensive review," *Int. Trans. Electr. Energy Syst.*, vol. 31, no. 11, p. e12580, 2020.
[5] E. A. Sciberras, B. Zahawi, and D. J. Atkinson, "Reducing shipboard emissions—Assessment of the role of electrical technologies," *Transp. Res. D, Transp. Environ.*, vol. 51, pp. 227–239, Mar. 2017.
[6] Y.-H. Hung, Y.-M. Tung, and C.-H. Chang, "Optimal control of integrated energy management/mode switch timing in a three-power-source hybrid powertrain," *Appl. Energy*, vol. 173, pp. 184–196, Jul. 2016.
[7] M. Soleymani, A. Yoosofi, and M. Kandi-D, "Sizing and energy management of a medium hybrid electric boat," *J. Mar. Sci. Technol.*, vol. 20, no. 4, pp. 739–751, Dec. 2015.
[8] S. East and M. Cannon, "Energy management in plug-in hybrid electric vehicles: Convex optimization algorithms for model predictive control," *IEEE Trans. Control Syst. Technol.*, vol. 28, no. 6, pp. 2191–2203, Nov. 2020.
[9] N. Planakis, G. Papalambrou, and N. Kyrtatos, "Predictive power-split system of hybrid ship propulsion for energy management and emissions reduction," *Control Eng. Pract.*, vol. 111, Jun. 2021, Art. no. 104795.
[10] H. Wang, J. Oncken, and B. Chen, "Receding horizon control for mode selection and powertrain control of a multi-mode hybrid electric vehicle," in *Proc. IEEE 90th Veh. Technol. Conf. (VTC-Fall)*, Honolulu, HI, USA, Sep. 2019, pp. 1–5.
[11] Y. Yuan, J. Wang, X. Yan, B. Shen, and T. Long, "A review of multi-energy hybrid power system for ships," *Renew. Sustain. Energy Rev.*, vol. 132, Oct. 2020, Art. no. 110081.
[12] K. Hein, Y. Xu, Y. Senthilkumar, W. Gary, and A. K. Gupta, "Rule-based operation task-aware energy management for ship power systems," *IET Gener., Transmiss. Distrib.*, vol. 14, no. 25, pp. 6348–6358, Dec. 2020.
[13] Y. Yuan, T. Zhang, B. Shen, X. Yan, and T. Long, "A fuzzy logic energy management strategy for a photovoltaic/diesel/battery hybrid ship based on experimental database," *Energies*, vol. 11, no. 9, p. 2211, Aug. 2018.
[14] G. Rinaldi, P. P. Menon, C. Edwards, and A. Ferrara, "Sliding mode observer-based finite time control scheme for frequency regulation and economic dispatch in power grids," *IEEE Trans. Control Syst. Technol.*, vol. 30, no. 3, pp. 1296–1303, May 2022.
[15] H. Abubakar, A. Muhammad, and S. Bello, "Ants colony optimization algorithm in the Hopfield neural network for agricultural soil fertility reverse analysis," *Iraqi J. Comput. Sci. Math.*, vol. 3, no. 1, pp. 32–42, 2022.
[16] A. R. Mayyas, S. Kumar, P. Pisu, J. Rios, and P. Jethani, "Model-based design validation for advanced energy management strategies for electrified hybrid power trains using innovative vehicle hardware in the loop (VHIL) approach," *Appl. Energy*, vol. 204, pp. 287–302, Oct. 2017.
[17] K. Ahn and S. Cha, "Developing mode shift strategies for a two-mode hybrid powertrain with fixed gears," *SAE Int. J. Passenger Cars-Mech. Syst.*, vol. 1, no. 1, pp. 285–292, 2009.
[18] R. A Hasan, S. Shahab Najim, and M. Abdullah Ahmed, "Correlation with the fundamental PSO and PSO modifications to be hybrid swarm optimization," *Iraqi J. Comput. Sci. Math.*, vol. 2, no. 2, pp. 25–32, 2021.
[19] A. Haseltalab, R. R. Negenborn, and G. Lodewijks, "Multi-level predictive control for energy management of hybrid ships in the presence of uncertainty and environmental disturbances," *IFAC-PapersOnLine*, vol. 49, no. 3, pp. 90–95, 2016.
[20] M. Kalikatzarakis, R. D. Geertsma, E. J. Boonen, K. Visser, and R. R. Negenborn, "Ship energy management for hybrid propulsion and power supply with shore charging," *Control Eng. Pract.*, vol. 76, pp. 133–154, Jul. 2018.
[21] X. Gao and L. Fu, "SOC optimization based energy management strategy for hybrid energy storage system in vessel integrated power system," *IEEE Access*, vol. 8, pp. 54611–54619, 2020.
[22] Z. Zhang, C. Guan, and Z. Liu, "Real-time optimization energy management strategy for fuel cell hybrid ships considering power sources degradation," *IEEE Access*, vol. 8, pp. 87046–87059, 2020.
[23] X. Wang, U. Shipurkar, A. Haseltalab, H. Polinder, F. Claeys, and R. R. Negenborn, "Sizing and control of a hybrid ship propulsion system using multi-objective double-layer optimization," *IEEE Access*, vol. 9, pp. 72587–72601, 2021.
[24] J. Mattingley, Y. Wang, and S. Boyd, "Receding horizon control," *IEEE Control Syst.*, vol. 31, no. 3, pp. 52–65, 2011.
[25] A. Ferrara, G. P. Incremona, and M. Cucuzzella, *Advanced and Optimization Based Sliding Mode Control: Theory and Applications*. Philadelphia, PA, USA: SIAM, 2019.
[26] W. Zhuang, X. Zhang, G. Yin, H. Peng, and L. Wang, "Mode shift schedule and control strategy design of multimode hybrid powertrain," *IEEE Trans. Control Syst. Technol.*, vol. 28, no. 3, pp. 804–815, May 2020.
[27] J. Oncken, K. Sachdeva, H. Wang, and B. Chen, "Integrated predictive powertrain control for a multimode plug-in hybrid electric vehicle," *IEEE/ASME Trans. Mechatronics*, vol. 26, no. 3, pp. 1248–1259, Jun. 2021.
[28] J. E. Whitesitt, *Boolean Algebra and Its Applications*. Chelmsford, MA, USA: Courier Corporation, 2012.
[29] R. Guerin and A. Orda, "Computing shortest paths for any number of hops," *IEEE/ACM Trans. Netw.*, vol. 10, no. 5, pp. 613–620, Oct. 2002.
[30] A. E. Brouwer and W. H. Haemers, "Distance-regular graphs," in *Spectra of Graphs*. New York, NY, USA: Springer, 2012, pp. 177–185.
[31] S. Delprat, J. Lauber, T. M. Guerra, and J. Rimaux, "Control of a parallel hybrid powertrain: Optimal control," *IEEE Trans. Veh. Technol.*, vol. 53, no. 3, pp. 872–881, May 2004.
[32] LMC Ltd. (2021). *LEM 200-Datasheet*. [Online]. Available: https://lynchmotors.co.U.K./pdfs/lmc-lem-200.pdf
[33] S. Kermani, S. Delprat, T. M. Guerra, R. Trigui, and B. Jeanneret, "Predictive energy management for hybrid vehicle," *Control Eng. Pract.*, vol. 20, no. 4, pp. 408–420, 2012.
[34] A. Rezaei, J. B. Burl, B. Zhou, and M. Rezaei, "A new real-time optimal energy management strategy for parallel hybrid electric vehicles," *IEEE Trans. Control Syst. Technol.*, vol. 27, no. 2, pp. 830–837, Mar. 2019.
[35] J. M. Maciejowski, *Predictive Control: With Constraints*. London, U.K.: Pearson, 2002.
[36] S. Even, *Graph Algorithms*. Cambridge, U.K.: Cambridge Univ. Press, 2011.

GIANMARIO RINALDI received the B.Sc. degree in energy engineering, the M.Sc. degree in electrical engineering, and the Ph.D. degree in control systems engineering from the University of Pavia, Italy, in 2014, 2016, and 2019, respectively. The design and successful validation (in sea) of an information driven optimal in-situ ocean sampling using gliders were accomplished during his NERC-funded postdoctoral research, from 2019 to 2021. He has been a Lecturer in clean powertrains with the Centre for Future Clean Mobility (CFCM), University of Exeter, since 2021. He is currently collaborating on Innovative U.K.-funded grants to develop clean solutions for marine applications and off-road heavy-duty vehicles. His expertises are in estimation, optimization, clean mobility, and energy networks. He is the author of 20 peer-reviewed articles in these areas, including nine journal publications and a book chapter.

PRATHYUSH P. MENON is currently an Associate Professor in control systems with the College of Engineering, Mathematics and Physical Sciences, University of Exeter, Exeter, U.K., where he is also the Deputy Director of the Centre for Future Clean Mobility. His current research interests include control, sliding mode observers, multiagent systems, energy networks, optimization, and simulation-based robustness analysis and uncertainty quantification. He has authored 100 refereed articles in these areas, including 40 journal publications.

RICHARD CREEK received the B.Eng. degree (Hons.) in mechanical engineering from The University of Sheffield and the M.Sc. degree in materials engineering from the University of Exeter, in 2020. He had an early career in software engineering and business analysis within corporate investment banking. He is currently a Research and Development Engineer leading an Innovate U.K. KTP Project at Lynch Motor Company, Devon, in partnership with the University of Exeter. His research interest includes engineering solutions to sustainability challenges faced by industry. The current KTP Project uses multiphysics simulation-driven design to develop the next generation of Lynch DC brushed axial flux electric motors targeting small passenger vessels in the marine sector. An additional focus is to collaborate on investigating options for diesel-electric hybrid solutions to provide a path toward full electrification of marine powertrains in support of the U.K.'s Maritime 2050 Zero-Emission Ambitions.